Appl. Phys. B (2015) 118:539–548
DOI 10.1007/s00340-015-6030-3

Applied Physics B
Lasers and Optics

Pulse repetition-frequency multiplication in a coupled cavity passively mode-locked semiconductor lasers

R. M. Arkhipov · A. Amann · A. G. Vladimirov

Received: 7 October 2014 / Accepted: 24 January 2015 / Published online: 15 February 2015

Abstract Using a delay differential equation model with two time delays, we investigate the dynamics of a semiconductor laser with an active cavity coupled to an external passive cavity. Our numerical simulations indicate that when the coupling between the two cavities is strong enough and the round-trip time of the active cavity is an integer multiple of the round-trip time of the external passive cavity, a harmonic mode-locking regime can develop in the laser with the pulse repetition period close to the passive cavity round-trip time. We also demonstrate that the output field intensity sensitively depends on the relative position of the frequency combs of the two cavities giving rise to a resonant behavior. The period and width of the resonances depend on the ratio of the round-trip times to the coupling between the two cavities. We show that the coupled cavity system under consideration can demonstrate a bistability between different regimes of generation.

R. M. Arkhipov (✉) · A. G. Vladimirov
Weierstrass Institute, Mohrenstr. 39, 10117 Berlin, Germany
e-mail: arkhipov@wias-berlin.de

R. M. Arkhipov
Faculty of Physics, St. Petersburg State University,
Ulyanovskaya 1, Petrodvoretz, 198504 St. Petersburg, Russia

R. M. Arkhipov
Humboldt-Universität zu Berlin, Mathematisch-Naturwissenschaftliche Fakultät, 12489 Berlin, Germany

A. Amann
School of Mathematical Sciences, University College Cork,
1.45 Western Gateway Building, Cork, Ireland

A. G. Vladimirov
Lobachevsky University of Nizhny Novgorod, Nizhny Novgorod, Russia

1 Introduction

Passively mode-locked semiconductor lasers generate short optical pulses with high repetition rates varying from few to hundreds of GHz. They have important applications in optical telecommunications, sampling, and division multiplexing [1–6]. Optical spectrum of these lasers is a frequency comb with the line spacing equal to the pulse repetition rate of the mode-locked regime. This repetition rate is limited by the fact that active medium length must be sufficiently large to achieve laser generation as well as by the operational frequencies of the optical modulators [7]. Therefore, different methods for pulse repetition frequency multiplication in such lasers have been used. Among them are the schemes employing colliding pulse mode-locking [8], the group delay dispersion in optical fibers (temporal fractional Talbot effect in optical fibers) [9, 10], chirped fiber Bragg grating based on the same Talbot effect [11, 12], and a number of uniform fiber Bragg gratings [7]. Another method of increasing the pulse repetition rate in a mode-locked laser is based on the use of a Fabry–Perot interferometer as an external spectral filter. This method is attractive due to its simplicity and robustness since commercially available Fabry–Perot filters may be employed [13, 14]. Experimentally it was realized by different authors, see for example, Refs. [13–17]. The idea of this method is the following [13]. If the separation between transmission peaks of the Fabry–Perot interferometer is exactly m times (m is an integer number) larger than the pulse repetition rate of the laser, then only those laser modes will be transmitted through the Fabry–Perot filter which coincide with the transmission lines of this filter. Since this leads to an increase in the separation between the resulting laser modes by m times, one can expect that the repetition frequency can be increased m times [13]. Typical

solid-state mode-locked femtosecond lasers have free spectral range from about 100 MHz to 1 GHz [18, 19]. On the other hand, for the precision measurements of astronomical objects, a comb spacing of 10–30 GHz is ideal [19]. This is why filtering of femtosecond-laser frequency combs by an external Fabry–Perot cavity is used to generate a broad spectrum of resolvable lines for astronomical measurements, for instance, in astronomical spectrograph calibration (see reviews [19–21]).

The problem of mode selection in single section semiconductor lasers is one of the most important problems in the control of laser radiation parameters [22]. In particular, semiconductor lasers with a fixed and predetermined number of primary modes are of interest for a number of applications. For example, two-color devices are useful for terahertz generation by photomixing [23]. In order to achieve a single-mode operation in Fabry–Perot semiconductor lasers, different methods have been used. In a distributed feedback laser, a Bragg grating in the active cavity can result in single-mode emission [24]. An alternative technique that can modify the lasing spectrum is the incorporation of a number of scattering centers in the form of slots into the laser cavity [25, 26]. This technique enables the design of single-mode lasers, two-mode lasers, or passively mode-locked discrete mode lasers [27, 28].

Furthermore, systems consisting of optically coupled lasers can exhibit a very rich variety of different dynamical phenomena and have much in common with other nonlinear systems [29–33]. For example, in optically coupled phase-locked lasers the break up of phase locking can lead to the appearance of chaotic dynamics [31]. The nonlinear dynamics in passively mode-locked semiconductor lasers is an active area of research nowadays [34]. In particular, in [35–39], the dynamics of passively mode-locked semiconductor lasers was studied theoretically using a system of delay differential equations (DDEs) model and experimentally. The dynamics of optically injected and hybrid mode-locked semiconductor lasers was considered, e.g., in [40, 41].

Optical bistability have been intensively investigated for decades because of its potential application in all-optical logic and signal processing, see, e.g., [42]. The existence of optical bistability in the system comprising a cavity mode and an ensemble of two-level atoms was demonstrated theoretically in [43]. It was shown that two stable CW regimes may coexist in this system and a hysteresis was observed between CW regimes when the frequency of the external harmonic signal was changed. Optical bistability was also studied theoretically and experimentally in optically injected semiconductor lasers [44], semiconductor lasers with optical feedback [45, 46], two coupled semiconductor lasers [47], optically injected two-section semiconductor lasers [48], and other laser systems.

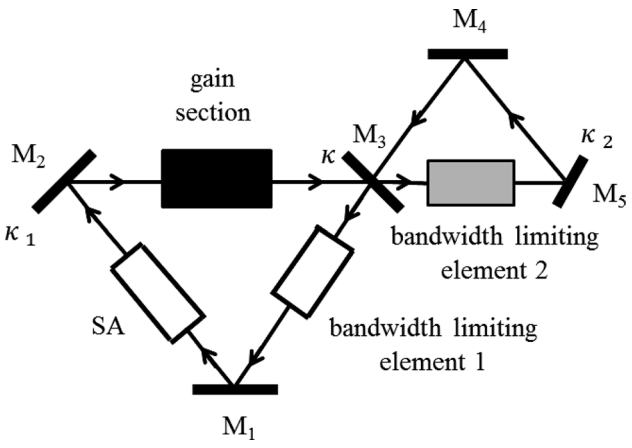

Fig. 1 Schematic representation of mode-locked laser coupled to a passive cavity. The active cavity contains gain section, saturable absorber section, and a spectral filtering element with the bandwidth γ_1. External passive cavity contains only a spectral filtering element with the bandwidth γ_2 which is assumed to be much larger than that of the active cavity, $\gamma_1 \ll \gamma_2$. Parameters κ, κ_1, and κ_2 are the reflectivities of the mirrors M_3, M_2, and M_5, respectively

Here using a DDE model, we study the dynamics of passively mode-locked semiconductor ring laser coupled to an external passive cavity. The external cavity in this case is used as a filter which suppresses certain longitudinal modes of the passively mode-locked laser. We demonstrate an increase in pulse repetition frequency f_p by a factor of 2 and 3 when the external cavity length is two and three times smaller than the active cavity. We study the dependence of mode-locked regimes on the model parameters and coupling coefficients between the two cavities. We demonstrate that changing the relative phase between the two electric fields in the two cavities leads to a periodic appearance of mode-locking windows with the pulse repetition rates $2f_p$ and $3f_p$, respectively. The period and width of these mode-locking windows depend on the passive cavity length.

Finally, we demonstrate the existence of optical bistability between a mode-locked regime and irregular pulsations in the model equations. We have found that a bistable behavior arises when the relative phase between electric fields in two cavities and the pumping power are changed.

2 Model equations

Our analysis is based on a set of DDE describing time evolution of the electric field amplitudes in the active cavity $A_1(t)$ and in the external cavity $A_2(t)$, as well as the saturable gain $G(t)$, and the saturable absorption $Q(t)$ in the gain and saturable absorber (SA) sections of the active cavity (see Fig. 1). This model is given by:

Table 1 Typical parameter values used in simulations

Spectral filtering bandwidth in the active cavity	γ_1	15
Spectral filtering bandwidth in the passive cavity	γ_2	50
Nonresonant field intensity attenuation factor per cavity round trip	$\kappa_1 = \kappa_2$	0.3
Linewidth enhancement factor in gain section	α_g	0
Linewidth enhancement factor in saturable absorber section	α_q	0
Pump parameter	g_0	0.5
Unsaturated absorption	q_0	2
Carrier relaxation rate in gain section	γ_g	0.01
Carrier relaxation rate in saturable absorber section	γ_q	1
Ratio of gain to absorber saturation intensities		10
Optical phase shift in the active cavity	ψ	0
Optical phase shift in the passive cavity	ϕ	0
Active cavity round-trip time	T_1	2.5
Passive cavity round-trip time	T_2	$T_1/2, T_1/3$

$$\frac{dA_1}{dt} = -\gamma_1 A_1 + \gamma_1\sqrt{\kappa}\sqrt{\kappa_1}e^{\frac{(1-i\alpha_g)G(t)-(1-i\alpha_q)Q(t)}{2}} A_1(t-T_1)e^{i\psi} + \gamma_1\sqrt{1-\kappa}\sqrt{\kappa_2}A_2(t-T_2)e^{i\phi}, \quad (1)$$

$$\frac{dA_2}{dt} = -\gamma_2 A_2 + \gamma_2\sqrt{1-\kappa}\sqrt{\kappa_1}e^{\frac{(1-i\alpha_g)G(t)-(1-i\alpha_q)Q(t)}{2}} A_1(t-T_1)e^{i\psi} + \gamma_2\sqrt{\kappa}\sqrt{\kappa_2}A_2(t-T_2)e^{i\phi}, \quad (2)$$

$$\frac{dG}{dt} = g_0 - \gamma_g G - e^{-Q}\left(e^G - 1\right)|A_1(t-T_1)|^2, \quad (3)$$

$$\frac{dQ}{dt} = \gamma_q(q_0 - Q) - s\left(1 - e^{-Q}\right)|A_1(t-T_1)|^2. \quad (4)$$

Here T_1 (T_2) is the round-trip time in the active (passive) cavity. The parameters ϕ and ψ describe the phase shifts of the fields A_1 and A_2 after the round trip in the active and passive cavity, respectively. Equations (1)–(4) generalize the model of a passively mode-locked semiconductor laser proposed in [35–37] to the case of two coupled cavities. DDE model proposed in [35–37] was derived from traveling wave equations (TWE) assuming the unidirectional propagation of light in the ring cavity. It was demonstrated in Refs. [38, 49, 50] that the results obtained within the framework of the DDE model are in agreement with those obtained using the TWE model. However, the DDE model does not take into account some effects related to counter-propagating waves interaction, which are important, e.g., in colliding pulse mode locking.

The parameters κ, κ_1, and κ_2 describe the reflectivities of the mirrors 3, 2, and 5, respectively, see Fig. 1. Typical values and a short description of the model parameters are given in Table 1. Each of the two coupled cavities has its own spectral filtering element. Since the passive cavity is empty, we assume that the spectral filtering bandwidth is much larger in the passive cavity than in the active one, $\gamma_2 \gg \gamma_1$. Below, for simplicity, we will consider the case when $\psi = 0$. The effect of the phase ϕ on the dynamics of coupled cavity laser is studied in Sect. 5. Let the active cavity round-trip time be equal to 25 ps. This corresponds to the pulse repetition frequency close to 40 GHz in the absence of external cavity and to $T_1 = 2.5$ in the normalized units of Eqs. (1)–(4) [37], where the time is normalized to the carrier relaxation time in the absorber section (10 ps).

3 Results of numerical simulations

3.1 80 GHz mode-locking regimes

In this section, we present the results of numerical simulations of Eqs. (1)–(4) with the parameter values given in Table 1. We demonstrate that when the external cavity length is approximately twice smaller than the laser cavity length, $T_2 \approx T_1/2$, an increase in the pulse repetition frequency by a factor of two can be achieved. First, we study the evolution of dynamical regimes with the increase in the reflectivity κ of the mirror 3. The bifurcation diagram in Fig. 2 shows the laser pulse peak intensity as a function of κ. To calculate this diagram, we have used the following procedure. At each given value of the parameter κ, Eqs. (1)–(4) have been integrated from $t = 0$ to $t = 5{,}000$ in order to skip the transient behavior. Next, during the time interval from $t = 5{,}000$ to $t = 7{,}000$, the maxima of the intensity time trace $|A_1(t)|^2$ have been plotted.

In Fig. 3, four different examples of the laser intensity time trace are given. When the reflectivity κ is small (strong coupling), the laser operates in a CW regime with the electric field intensity independent of time. The intensity time trace illustrating this regime is shown in Fig. 3a.

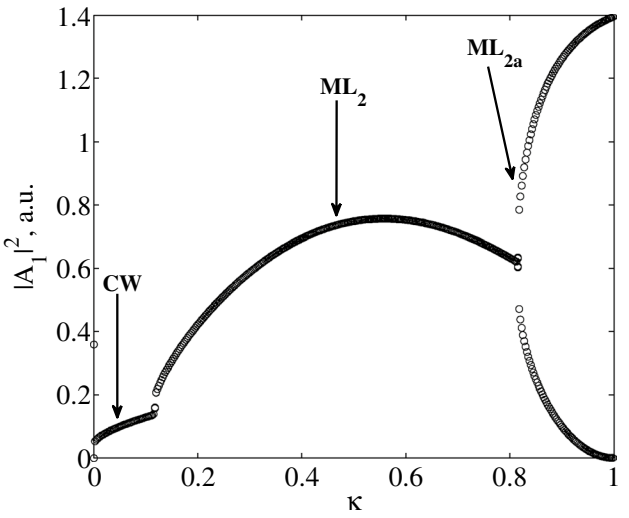

Fig. 2 Bifurcation diagram presenting the sequence of dynamical regimes taking place with the increase in the reflectivity κ. $T_2 = T_1/2$, other parameter values are given in Table 1. CW, ML_2, and ML_{2a} indicate continuous wave, 80 GHz mode-locking regime, and 80 GHz mode-locking regime with two pulses in the cavity having different peak powers, respectively

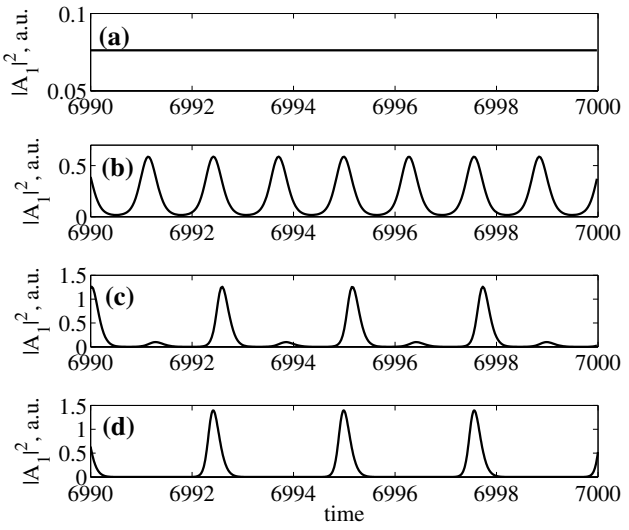

Fig. 3 Intensity time traces at different values of the reflectivity parameter κ. **a** CW regime, $\kappa = 0.02$, **b** 80 GHz mode-locking $ML_2, \kappa = 0.3$, **c** harmonic mode-locking regime with two pulses having different peak powers $ML_{2a}, \kappa = 0.9$, **d** 40-GHz fundamental ML regime, $\kappa = 1$

This regime is indicated as CW in Fig. 2. An increase in κ leads to the appearance a harmonic mode-locking regime (ML_2) with the pulse repetition frequency close to 80 GHz (see Fig. 3b). In this regime, the laser emits two pulses per active cavity round-trip time T_1. The peak intensity of these pulses increases with κ for $\kappa \leq 0.5$. Further increase in the

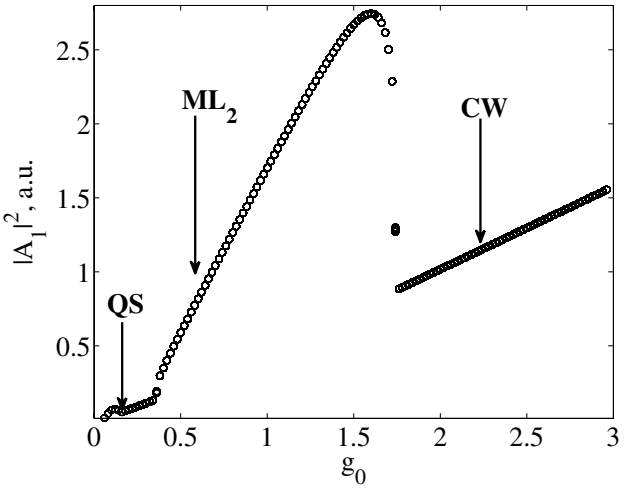

Fig. 4 Pulse peak power $|A_1|^2$ versus $g_0, \kappa = 0.3$ and $T_2 = T_1/2$. Other parameter values are given in Table 1. Q-switching regime shown in Fig. 5 is indicated as *QS*

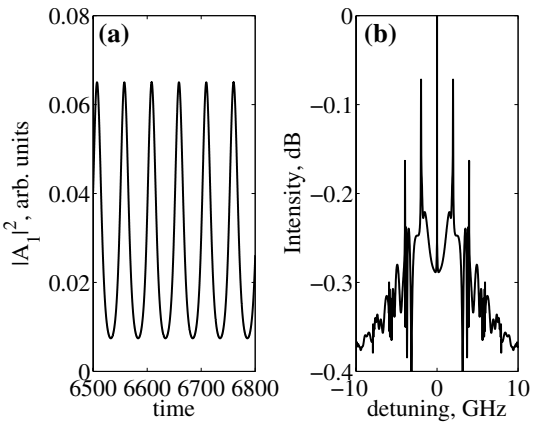

Fig. 5 Q-switching regime (QS) for $g_0 = 0.1$ and $\kappa = 0.3$. **a** laser intensity time trace, **b** optical spectrum. Other parameter values are the same as in Fig. 4

reflectivity κ up to 0.8 leads to a decrease in the pulse peak intensity. When κ becomes larger than 0.8, a transition to a regime ML_{2a} with two pulses in the cavity having different peak intensities takes place via a period doubling bifurcation (Fig. 3c). One of these pulses has a larger pulse peak power and the other smaller than the peak power of the harmonic mode-locking regime with two identical pulses shown in Fig. 3b. Finally, at large coupling strengths $\kappa = 1$, the laser undergoes a transition to fundamental mode-locking regime with the repetition frequency 38.88 GHz, see Fig. 3d.

Figure 4 has been obtained in a similar way as Fig. 2, but with the linear gain, g_0 taken as a bifurcation parameter instead of κ. As it is seen from Fig. 4, when the linear gain g_0 is small enough, the laser exhibits a Q-switching

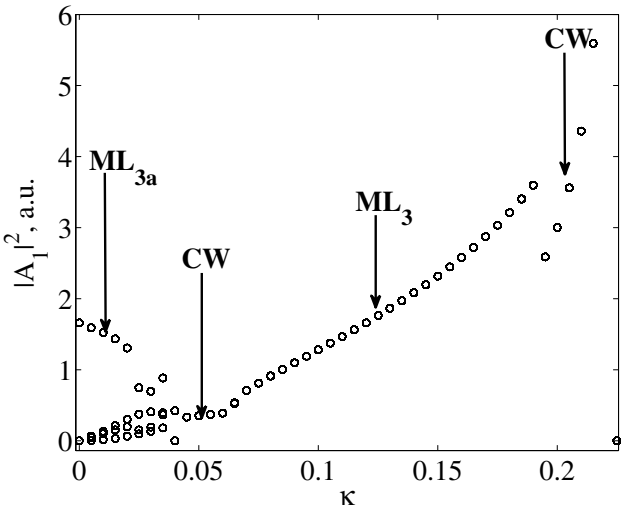

Fig. 6 Bifurcation diagram illustrating pulse peak power $|A_1|^2$ as a function of reflectivity $\kappa, T_2 = T_1/3, q_0 = 3, \kappa_1 = 0.3$, and $\kappa_2 = 0.9$. Other parameter values are given in Table 1. Mode-locking regimes with three pulses in the cavity having different peak powers are indicated ML_{3a}. Intensity time trace of this regime is shown in Fig. 7a, b. ML_3 indicates harmonic mode-locking regime with the pulse repetition rate close to 120 GHz, see Fig. 7d

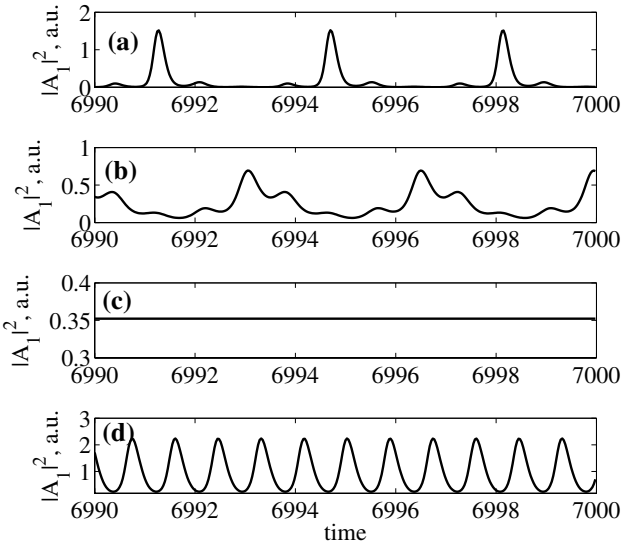

Fig. 7 Laser intensity time traces for different values of the reflectivity κ. **a** ML_{3a} regime of periodic pulsations with the period determined by the sum of the round-trip times of the two cavities, $2T_1/3, \kappa = 0.01$, **b** ML_{3a} regime, $\kappa = 0.03$, **c** CW regime, $\kappa = 0.05$, **d** 120 GHz mode-locking regime $ML_3, \kappa = 0.15$. Other parameter values are the same as in Fig. 6

regime QS with the laser intensity oscillating at a low frequency (around 2 GHz), which is approximately one order of magnitude smaller than the pulse repetition frequency f_p of the fundamental mode-locking regime. The corresponding time trace and power spectrum are presented in Fig. 5. Q-switching regimes in passively mode-locked quantum dot lasers were studied theoretically using a DDE model in [39]. For $0.161 < g_0 < 0.361$, the laser operates in a CW regime. With further increase in the pump parameter g_0, a transition to a harmonic mode-locking regime with approximately twice higher repetition rate appears. This regime is similar to that shown in Fig. 3b. Finally, for $g_0 > 1.5$, a CW regime becomes stable.

3.2 120-GHz mode-locking regimes

In this subsection, we study the dynamics of a passively mode-locked semiconductor laser coupled to a passive cavity of length $L/3$, where L is the active cavity length ($T_2 = T_1/3$). In the simulations, we have used the parameter values $q_0 = 3, \kappa_1 = 0.3$, and $\kappa_2 = 0.9$. Other parameter values are given in Table 1. Similarly to the case discussed in the previous section, when the coupling strength κ is large enough, one can expect the appearance of harmonic mode-locking regime with "multiplied" pulse repetition frequency $3f_p$. Such regimes were observed in numerical simulations of a DDE model of solitary passively mode-locked semiconductor laser without external cavity ($\kappa = 1$) at sufficiently large values of the pumping parameter g_0 [37].

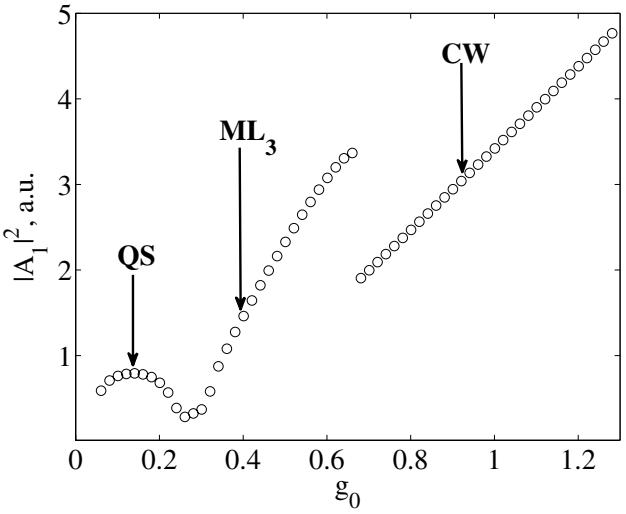

Fig. 8 Pulse peak power $|A_1|^2$ versus $g_0, T_2 = T_1/3, \kappa = 0.15, \kappa_1 = 0.3$, and $\kappa_2 = 0.9$. Other parameters are the same as in Fig. 6

Bifurcation diagram illustrating the dependence of the pulse peak power $|A_1|^2$ on the reflectivity κ is presented in Fig. 6. When $\kappa < 0.05$, the laser exhibits periodic pulsations (ML_{3a}) with the period close to $2T_1/3$ determined by the sum of the lengths of the two cavities. Two intensity time traces of this regime corresponding to $\kappa = 0.01$ and $\kappa = 0.03$ are plotted in Fig. 7a, b. At slightly larger reflectivities, the laser starts to operate in a CW regime (see Fig. 7c). Then, when κ becomes close to 0.07, harmonic

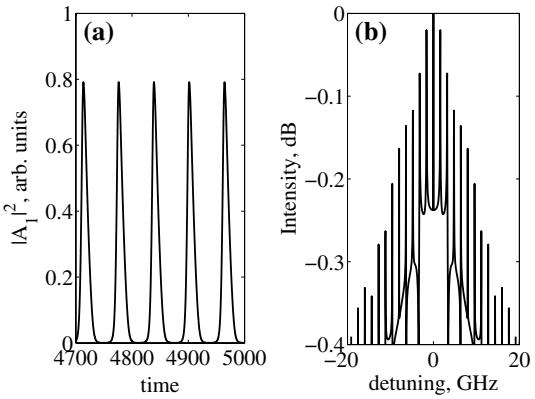

Fig. 9 **a** Intensity time traces illustrating Q-switching regime for $g_0 = 0.14$. **b** Optical spectrum. $T_2 = T_1/3, \kappa = 0.15, \kappa_1 = 0.3, \kappa_2 = 0.9$. Other parameters are the same as in Fig. 8

mode-locking regime with the "multiplied" pulse repetition frequency close to $3f_p$ appears. The field intensity time trace for this regime is shown in Fig. 7d. Finally, at sufficiently large κ, a transition from the harmonic mode-locking regime to a CW regime takes place.

To study the effect of the injection current on the harmonic mode-locking regime with the pulse repetition frequency $3f_p$, in Fig. 8, we present a bifurcation diagram illustrating the dependence of pulse peak power $|A_1|^2$ on the pump parameter g_0. This figure corresponds to the fixed value of the reflectivity $\kappa = 0.15$, for which this regime occurs in Fig. 6. When g_0 is small enough, the laser operates in Q-switching (QS) regime (see Fig. 9), which corresponds to a periodic pulse train with the pulse peak power oscillating at low frequency close to 1.7 GHz. At larger g_0 close to 0.3 harmonic mode-locking regime with the pulse repetition frequency close to $3f_p$ (ML_3) appears, as it is seen in Fig. 7d. Finally, for $g_0 > 0.66$, a CW regime becomes stable.

Our analysis indicates that the harmonic mode-locking regimes with the pulse repetition rate $3f_p$ can be observed not only in the case when the passive cavity is three times shorter than the active one $T_2 = T_1/3$, but also for $T_2 = 2T_1/3$. In both cases, every third mode of the active cavity coincides with a certain mode of the external passive cavity, and hence, the mode-locking regimes with the pulse repetition rate $3f_p$ can be expected. Bifurcation diagram obtained for the case $T_2 = 2T_1/3$ is similar to that shown in Fig. 6.

4 Nonzero linewidth enhancement factors

In this subsection, we study the effect of the linewidth enhancement factors on the dynamics of Eqs. (1)–(4). It

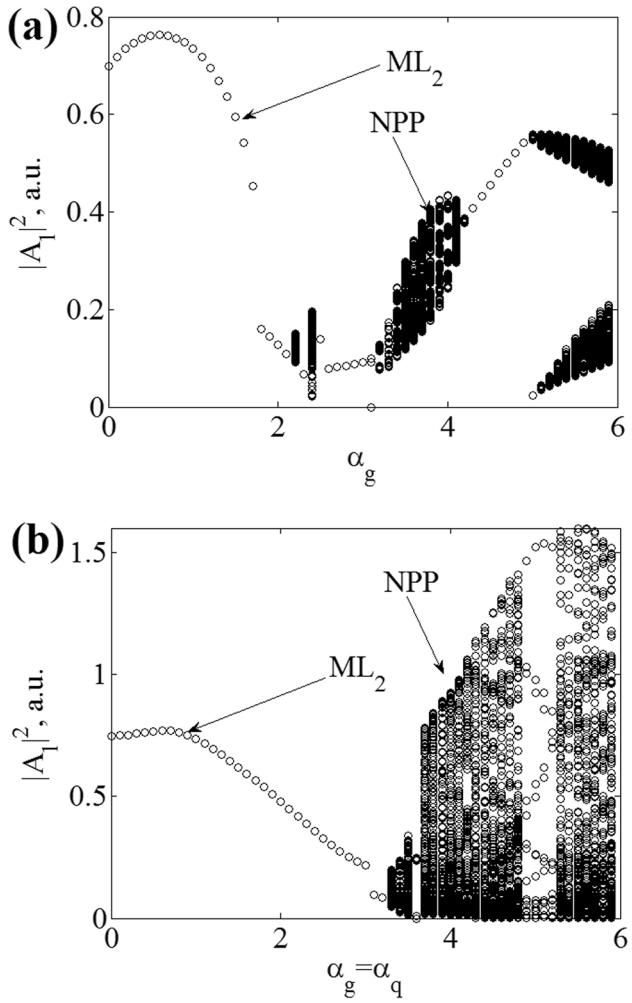

Fig. 10 Bifurcation diagrams obtained by changing the linewidth enhancement factors α_g and α_q. $T_2 = T_1/2$. **a** Pulse peak power versus $\alpha_g, \alpha_q = 1.0$, **b** pulse peak power versus $\alpha_g = \alpha_q, \kappa = 0.5$. Other parameters are given in Table 1

is known that for sufficiently large linewidth enhancement factors, mode-locking regime can be destabilized and irregular pulsations can appear. The influence of the α-factors on the dynamics of passively mode-locked semiconductor laser without external cavity was studied in [37]. Figure 10 was obtained by taking the linewidth enhancement factors as bifurcation parameters. It is seen from Fig. 10a corresponding to $\alpha_q = 1.0$ that the largest pulse peak powers were observed in the case when the linewidth enhancement factors in the two sections are approximately equal: $\alpha_g \approx \alpha_q$. This can be intuitively explained as follows [37]. Since gain and loss enter in Eq. (1) with opposite signs, the contributions of the gain and absorption sections into the pulse chirp must compensate each other, at least partially, when the two linewidth enhancement factors have the same sign. When α_g is increased, the pulse peak power decreases and a transition to irregular pulsations and CW regime

takes place (starting from $\alpha_g \simeq 1.7$). Similar behavior was observed for $\alpha_g = \alpha_q$, see Fig. 10b: The pulse peak power decreases with the increase in the two linewidth enhancement factors and a transition to regime with irregular pulsations takes place at $\alpha_g = \alpha_q \simeq 3$. It was found in [37] that this transition is associated with the intermittency between mode-locking solution and irregular intensity pulsations. Slightly above the transition point, time intervals characterized by almost regular mode-locking behavior alternate with irregular spiking. The duration of the "regular" time intervals decreases with the increase in α_g, and finally, a regime with irregular pulsations develops. The break up of mode-locking regime can be explained by the presence of intracavity dispersion. When the linewidth enhancement factors are large, frequencies of the laser modes become nonequidistant due to the strong intracavity dispersion, and mode-locking regime disappears.

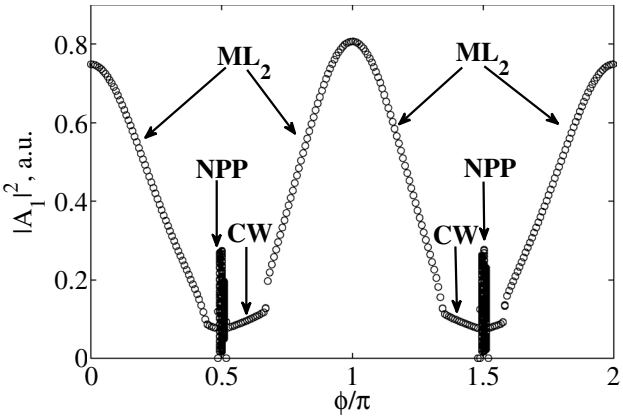

Fig. 11 Pulse peak power $|A_1|^2$ versus ϕ. $\kappa = 0.5, \kappa_1 = 0.3, \kappa_2 = 0.3$, and $T_2 = T_1/2$. Other parameters are given in Table 1. NPP indicates a regime with nonperiodic pulsations of the electric field, see Fig. 12b

5 Influence of the relative phase ϕ

In the previous section, we assumed that the phase shifts in both cavities are equal to zero, $\phi = \psi = 0$. This means that the frequency of the central mode of the active cavity coincides with that of the passive cavity. In order to satisfy this condition, it is necessary to make optical length of the external cavity n times smaller than the optical length of the active cavity ($L_2 = L_1/n, n$-integer number) with the precision of a small fraction of a wavelength. However, since in reality it is rather difficult to build the two cavities with such a high precision, it is interesting to consider the dynamics of the coupled cavity laser in the case when the central mode of the passive cavity is shifted in frequency with respect to that of the active cavity, $\phi \neq 0$. To this end, we take the phase ϕ as the bifurcation parameter and perform numerical integration of the model Eqs. (1)–(4) with the parameters given in Table 1, $T_2 = T_1/2$, and $\kappa = 0.5$. Bifurcation diagram illustrating the dependence of the pulse peak power $|A_1|^2$ on the parameter ϕ is presented in Fig. 11. It is seen that this dependence has a multi-resonant character and is periodic with the period 2π. This periodicity can be easily understood by taking into account the invariance of Eqs. (1)–(2) under the transformation $\phi \to \phi + 2\pi$. In Fig. 11, the values of ϕ characterized by a single-valued pulse peak power (peak powers of all pulses in the intensity time trace are equal, see Fig. 12a) correspond to mode-locking regimes with the pulse repetition frequency close to $2f_p$. The pulse peak power of this regime achieves its maximums at $\phi = k\pi$ with $k = 0, \pm 1, \pm 2 \ldots$. Finally, near $\phi = (1/2 + k)\pi$ regimes with nonperiodic pulsations of the pulse peak power are observed. The intensity time traces of these regimes corresponding to a cloud of points in Fig. 11 are shown in Fig. 12b for $\phi = \frac{\pi}{2}$.

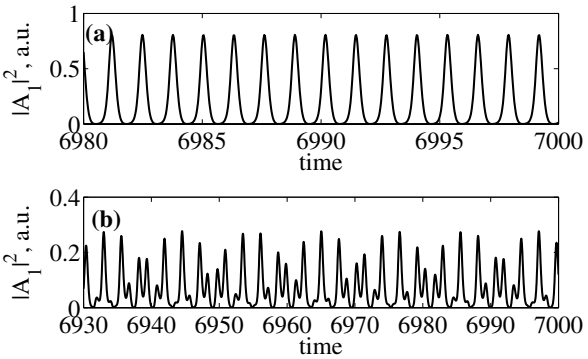

Fig. 12 Intensity time traces $|A_1(t)|^2$ calculated for different values of the parameter ϕ. **a** 80 GHz mode-locking, $\phi = \pi$, **b** regime of nonperiodic pulsations NPP, $\phi = 0.5\pi$. $\kappa_1 = \kappa_2 = 0.3, \kappa = 0.5$, and $T_2 = T_1/2$. Other parameter values are given in Table 1

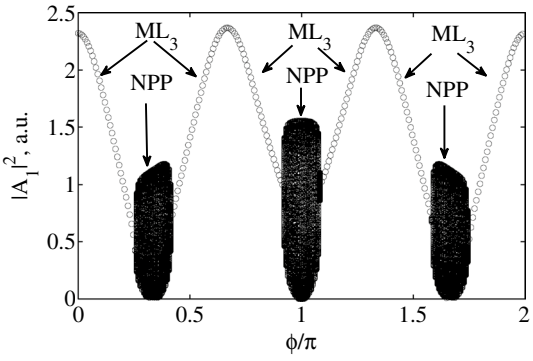

Fig. 13 Bifurcation diagram of the pulse peak power $|A_1|^2$ versus ϕ. $\kappa = 0.15, \kappa_1 = 0.3, \kappa_2 = 0.9$, and $T_2 = T_1/3$). Other parameter values are given in Table 1

Resonant behavior similar to that presented in Fig. 11 was observed in the case $T_2 = T_1/3$ as well, see Fig. 13. However, in this case, the maximal pulse peak power of the harmonic mode-locking regime at $\phi = \frac{2\pi k}{3}, k = 0, \pm 1, \pm 2 \ldots$ is larger than that in the case $T_2 = T_1/2$, and the windows of nonperiodic pulsations are located around $\phi = \frac{(2k+1)\pi}{3}, k = 0, \pm 1, \pm 2 \ldots$. The nonperiodic regimes appear as a result of destabilization of harmonic mode-locking due to the interference between the electric fields in the two cavities. Note that the resonant behavior shown Fig. 11 is similar to the dependence of the transmission function of a Fabry–Perot cavity on the relative phase ϕ [51].

6 Optical bistability

Bistable devices are important in the field of optical signal processing. They can be used as optical logic elements. In the present section, we demonstrate the appearance of optical bistability in the model Eqs. (1)–(4). We consider the case of nonzero linewidth enhancement factors in the gain and absorber sections, $\alpha_g = 3$ and $\alpha_q = 1$. Fig. 14 shows the dependence of the pulse peak power $|A_1|^2$ on the phase ϕ for $T_2 = T_1/3$. This figure was obtained by numerical integration of the model equations at each value of the parameter ϕ on an equidistant grid with the solution calculated at the previous value of ϕ taken as an initial condition. After the integration, the pulse peak powers plotted versus the phase ϕ. This procedure was repeated with stepwise increasing and stepwise decreasing of the phase parameter ϕ. Black circles and red crosses in Fig. 14 correspond to the case when the parameter ϕ was increased and decreased, respectively. It is seen from the figure that within the intervals $0.64\pi < \phi < 0.74\pi$ and $1.3\pi < \phi < 1.4\pi$, the laser exhibits a bistability between harmonic mode-locked states (ML_3) with the repetition rate close to 120 GHz and nonperiodic regimes (NPP). Furthermore, our simulations indicate that the appearance of optical bistability in the system is related to nonzero linewidth enhancement factors in the gain and absorber sections.

In typical experiments on optical bistability, the laser output power is measured as a function of the injection current [45–47]. The diagram shown in Fig. 15 was obtained in similar way as Figs. 4 and 8, but with the pump parameter g_0 taken as a bifurcation parameter instead of the detuning ϕ. It corresponds to the case when the external cavity length is three times smaller than that of the active cavity, $T_2 = T_1/3$. It is seen from this figure that when the pump parameter is small, the laser operates in Q-switching regime (QS). With the increase in g_0, a transition to harmonic mode-locking regime with the pulse repetition rate close to $3f_p$ (ML_{3f}) takes place, see black circles in Fig. 15. Finally, at $g_0 \approx 1.5$, the laser starts to operate in

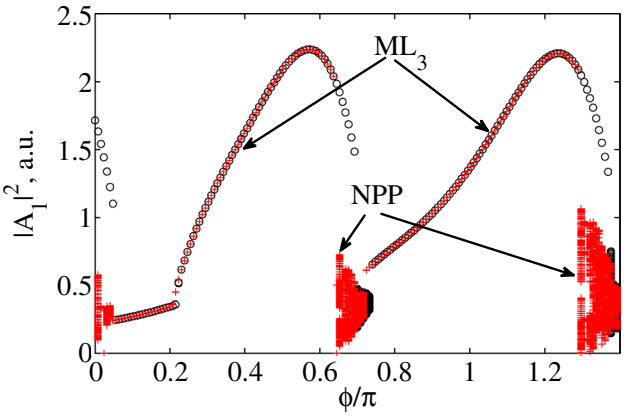

Fig. 14 Bifurcation diagram of the pulse peak power $|A_1|^2$ versus ϕ. $q_0 = 3, \kappa = 0.15, \kappa_1 = 0.3, \kappa_2 = 0.9, T_2 = T_1/3, \alpha_g = 3$, and $\alpha_q = 1$. *Black circles* (*red crosses*) correspond to the case when ϕ was increased (decreased). Other parameter values are given in Table 1

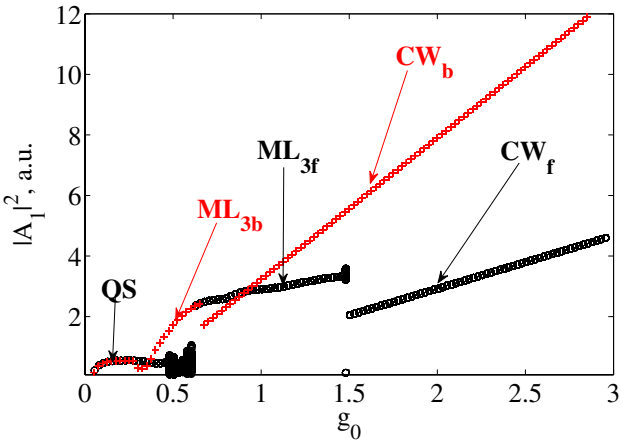

Fig. 15 Bifurcation diagram of the pulse peak power $|A_1|^2$ versus pump parameter g_0. $q_0 = 3, \kappa = 0.15, \kappa_1 = 0.3, \kappa_2 = 0.9, T_2 = T_1/3, \alpha_g = 3, \alpha_q = 1$, and $\phi = 0$. *Black circles* (*red crosses*) correspond to the case when g_0 was increased (decreased). Other parameter values are given in Table 1. CW_f and CW_b indicate two bistable CW regimes. ML_{3f} and ML_{3b} correspond to harmonic mode-locking regimes with the pulse repetition frequency close to 120 GHz

CW regime (CW_f). When the pump parameter is decreased (red crosses in Fig. 15), the laser starts from a CW regime (CW_b in Fig. 15), but the electric field intensity in this case is larger than that of the regime CW_f. The regime CW_b is stable for $g_0 \gtrsim 0.65$. Below this value, a transition to a harmonic mode-locking regime with the frequency close to $3f_p$ (ML_{3b}) takes place. Further decrease in g_0 leads to the transition to Q-switching regime QS coinciding with that obtained by increasing g_0.

Physical mechanisms responsible for the appearance of bistability can be different. For example, it was

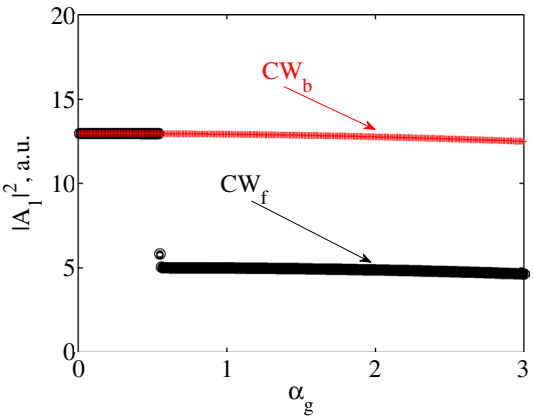

Fig. 16 Bifurcation diagram of the pulse peak power $|A_1|^2$ versus α_g. $g_0 = 2.98$. Other parameter values are the same as in Fig. 15

demonstrated in Ref. [47] that bistability in two coupled semiconductor lasers arises due to the gain saturation that is strongly affected by the mutual coupling of the two cavities.

To demonstrate that the bistability shown in Fig. 15 is related to the presence of the nonzero linewidth enhancement factors in the model equations, we integrated these equations with α_g taken as a bifurcation parameter and $g_0 = 2.98$, see Fig. 16. Red crosses and black circles were obtained by decreasing and increasing the parameter α_g from $\alpha_g = 3$ to $\alpha_g = 0$ along the branches CW_b and CW_f, respectively, see Fig. 15. The result of these simulations is plotted in Fig. 16. It is seen from Fig. 16 that two stable CW branches coexist for $\alpha_g < \alpha_g^* \approx 0.55$. However, at small $\alpha_g < \alpha_g^*$, the branch CW$_f$ with smaller laser intensity becomes unstable and bistability disappears.

7 Conclusions

In conclusion, we have studied the dynamics of a 40-GHz passively mode-locked semiconductor laser coupled to an external passive cavity. Our analysis was based on a set of DDEs governing the time evolution of the electric field envelopes in the two cavities, saturable gain, and saturable absorption. We have shown that the dynamical behavior of the laser depends strongly on the length of the external cavity, the coupling strength between the two cavities, pumping parameter, and the relative phase ϕ. If the length of the external cavity is two or three times smaller than that of the active cavity and the coupling between two cavities is strong enough, it is possible to generate mode-locking pulses with the "multiplied" repetition frequency close to $2f_p$ or $3f_p$, respectively.

We have investigated the effect of the linewidth enhancement factors on a coupled cavity mode-locked laser dynamics. In particular, our numerical simulations indicate that at large linewidth enhancement factors, mode-locking regimes with the pulse repetition rates $2f_p$ and $3f_p$ can be destroyed, and as a result, irregular pulsations can develop. Break up of the mode-locking regimes can be attributed to the intermode distance variation due to the intracavity dispersion.

We have studied the effect of the phase ϕ describing the relative position of the frequency combs associated with active and passive cavity on the system behavior. Numerical simulations indicate that the pulse peak power has a periodic dependence on ϕ, and there is a transition between nonperiodic and mode-locking regimes when ϕ changes. This periodic dependence seems to have the similar nature as the dependence of the transmission function of a Fabry–Perot cavity on the electric field phase.

We have demonstrated the existence of optical bistability between different laser operation regimes. The bistability arises only when the linewidth enhancement factors are nonzero in the gain and the saturable absorber sections. At zero or sufficiently small linewidth enhancement factors, no bistability was observed in our numerical simulations.

Acknowledgments R.M.A. and A.G.V. would like to acknowledge the support of EU FP7 ITN PROPHET, Grant No. 264687. A.G.V. acknowledges the support of the SFB 787, E.T.S. Walton Visitors Award of the Science Foundation Ireland, and of the grant 14-41-00044 of RFS. Authors are grateful to M. Radziunas and I. Kashchenko for helpful discussions.

References

1. D. Bimberg, M. Grundmann, N.N. Ledentsov, *Quantum Dot Heterostructures* (Wiley, Chichester, 1999). ISBN:978-0-471-97388-1
2. D. Bimberg, Quantum dot based nanophotonics and nanoelectronics. Electron. Lett. **44**, 168–171 (2008)
3. E.U. Rafailov, M.A. Cataluna, Mode-locked quantum-dot lasers. Nat. Photonics **1**, 395–401 (2007)
4. E.U. Rafailov, M.A. Cataluna, E.A. Avrutin, *Ultrafast Lasers Based on Quantum-Dot Structures: Physics and Devices* (Wiley, New York, 2011)
5. P.G. Kryukov, Ultrashort-pulse lasers. Quantum Electron. **31**(2), 95–119 (2001)
6. P.G. Kryukov, Continuous-wave femtosecond lasers. Phys. Uspekhi **183**, 897–916 (2013)
7. N.K. Berger, B. Levit, S. Atkins, B. Fischer, Repetition-rate multiplication of optical pulses using uniform fiber Bragg gratings. Opt. Commun. **221**(4), 331–335 (2003)
8. R. Fork, B. Greene, C. Shank, Generation of optical pulses shorter than 0.1 psec by colliding pulse mode locking. Appl. Phys. Lett. **38**(9), 671–672 (1981)
9. M.H. Takara, S. Kawanishi, High-repetition-rate optical pulse generation by using chirped optical pulses. Electron. Lett. **34**, 792–793 (1998)
10. S. Arahira, S. Kutsuzawa, Y. Matsui, D. Kunimatsu, Y. Ogawa, Repetition-frequency multiplication of mode-locked pulses using fiber dispersion. J. Lightwave Technol. **16**(3), 405–410 (1998)

11. S. Longhi, M. Marano, P. Laporta, O. Svelto, M. Belmonte, B. Agogliati, L. Arcangeli, V. Pruneri, M. Zervas, M. Ibsen, 40-GHz pulse-train generation at 1.5 μm with a chirped fiber grating as a frequency multiplier. Opt. Lett. **25**(19), 1481–1483 (2000)
12. J. Azana, M.A. Muriel, Technique for multiplying the repetition rates of periodic trains of pulses by means of a temporal self-imaging effect in chirped fiber gratings. Opt. Lett. **24**(23), 1672–1674 (1999)
13. T. Sizer et al., Increase in laser repetition rate by spectral selection. IEEE J. Quantum Electron. **25**(1), 97–103 (1989)
14. K. Yiannopoulos, K. Vyrsokinos, D. Tsiokos, E. Kehayas, N. Pleros, G. Theophilopoulos, T. Houbavlis, G. Guekos, H. Avramopoulos, Pulse repetition frequency multiplication with spectral selection in Fabry–Perot filters. IEEE J. Quantum Electron. **40**(2), 157–165 (2004)
15. U. Keller, W.H. Knox, H. Roskos, Coupled-cavity resonant passive mode-locked Ti: sapphire laser. Opt. Lett. **15**(23), 1377–1379 (1990)
16. D.K. Serkland, G.D. Bartolini, W.L. Kath, P. Kumar, A.V. Sahakian, Rate multiplication of a 59-GHz soliton source at 1550 nm. J. Lightwave Technol. **16**(4), 670–677 (1998)
17. M. Kirchner, D. Braje, T. Fortier, A. Weiner, L. Hollberg, S. Diddams, Generation of 20 GHz, sub-40 fs pulses at 960 nm via repetition-rate multiplication. Opt. Lett. **34**(7), 872–874 (2009)
18. W. Sibbett, A. Lagatsky, C. Brown, The development and application of femtosecond laser systems. Opt. Express **20**(7), 6989–7001 (2012)
19. D. Braje, M. Kirchner, S. Osterman, T. Fortier, S. Diddams, Astronomical spectrograph calibration with broad-spectrum frequency combs. Eur. Phys. J. D **48**(1), 57–66 (2008)
20. Z. Jiang, C.B. Huang, D.E. Leaird, A.M. Weiner, Optical arbitrary waveform processing of more than 100 spectral comb lines. Nat. Photonics **1**(8), 463–467 (2007)
21. T. Steinmetz, T. Wilken, C. Araujo-Hauck, R. Holzwarth, T.W. Hänsch, L. Pasquini, A. Manescau, S. D'Odorico, M.T. Murphy, T. Kentischer et al., Laser frequency combs for astronomical observations. Science **321**(5894), 1335–1337 (2008)
22. P. Smith, Mode selection in lasers. Proc. IEEE **60**(4), 422–440 (1972)
23. M. Tani, O. Morikawa, S. Matsuura, M. Hangyo, Generation of terahertz radiation by photomixing with dual-and multiple-mode lasers. Semicond. Sci. Technol. **20**(7), S151 (2005)
24. L.A. Coldren, S.W. Corsine, *Diode Lasers and Photonic Integrated Circuits* (Wiley, New York, 1995)
25. B. Corbett, D. McDonald, Single longitudinal mode ridge waveguide 1.3 μm Fabry–Perot laser by modal perturbation. Electron. Lett. **31**(25), 2181–2182 (1995)
26. S. O'Brien, A. Amann, R. Fehse, S. Osborne, E.P. O'Reilly, J.M. Rondinelli, Spectral manipulation in Fabry–Perot lasers: perturbative inverse scattering approach. JOSA B **23**(6), 1046–1056 (2006)
27. S. Osborne, S. O'Brien, K. Buckley, R. Fehse, A. Amann, J. Patchell, B. Kelly, D.R. Jones, J. O'Gorman, E.P. O'Reilly, Design of single-mode and two-color Fabry–Perot lasers with patterned refractive index. IEEE J. Sel. Top. Quantum Electron. **13**(5), 1157–1163 (2007)
28. S. O'Brien, S. Osborne, D. Bitauld, N. Brandonisio, A. Amann, R. Phelan, B. Kelly, J. O'Gorman, Optical synthesis of terahertz and millimeter-wave frequencies with discrete mode diode lasers. IEEE Trans. Microw. Theory Tech. **58**(11), 3083–3087 (2010)
29. A. Glova, Phase locking of optically coupled lasers. Quantum Electron. **33**(4), 283–306 (2003)
30. R.Z. Sagdeev et al., *Nonlinear Physics: From the Pendulum to Turbulence and Chaos* (Harwood, Chur, 2008)
31. H. Haken, *Laser Light Dynamics* (North-Holland Pub. Co, Amsterdam, 1985)
32. H.E. Hagemeier, S.R. Robinson, Field properties of multiple coherently combined lasers. Appl. Opt. **18**(3), 270–280 (1979)
33. M.B. Spencer, W.E. Lamb, Theory of two coupled lasers. Phys. Rev. A **5**(2), 893 (1972)
34. E. Avrutin, J. Marsh, E. Portnoi, Monolithic and multi-gigahertz mode-locked semiconductor lasers: constructions, experiments, models and applications, in *IEE Proceedings-Optoelectronics*, vol. 147, (IET, 2000), pp. 251–278
35. A.G. Vladimirov, D. Turaev, A new model for a mode-locked semiconductor laser. Radiophys. Quantum Electron. **47**(10–11), 769–776 (2004)
36. A. G. Vladimirov, D. Turaev, G. Kozyreff. Delay differential equations for mode-locked semiconductor lasers. Opt. Lett. **29**(11), 1221–1223 (2004)
37. A.G. Vladimirov, D. Turaev, Model for passive mode locking in semiconductor lasers. Phys. Rev. A **72**(3), 033808 (2005)
38. A.G. Vladimirov, A.S. Pimenov, D. Rachinskii, Numerical study of dynamical regimes in a monolithic passively mode-locked semiconductor laser. IEEE J. Quantum Electron. **45**(5), 462–468 (2009)
39. A.G. Vladimirov, U. Bandelow, G. Fiol, D. Arsenijević, M. Kleinert, D. Bimberg, A. Pimenov, D. Rachinskii, Dynamical regimes in a monolithic passively mode-locked quantum dot laser. JOSA B **27**(10), 2102–2109 (2010)
40. N. Rebrova, G. Huyet, D. Rachinskii, A.G. Vladimirov, Optically injected mode-locked laser. Phys. Rev. E **83**, 066202 (2011)
41. R. Arkhipov, A. Pimenov, M. Radziunas, D. Rachinskii, A.G. Vladimirov, D. Arsenijevic, H. Schmeckebier, D. Bimberg, Hybrid mode locking in semiconductor lasers: simulations, analysis, and experiments. IEEE J. Sel. Top. Quantum Electron. **19**(4), 1100208–1100208 (2013)
42. H. Gibbs, *Optical Bistability: Controlling Light with Light* (Elsevier, Amsterdam, 1985)
43. A.N. Oraevsky, Resonant properties of a system comprising a cavity mode and two-level atoms and frequency bistability. Quantum Electron. **29**(11), 975–978 (1999)
44. T. Erneux, E.A. Viktorov, B. Kelleher, D. Goulding, S. Hegarty, G. Huyet, Optically injected quantum-dot lasers. Opt. Lett. **35**(7), 937–939 (2010)
45. P. Glas, R. Müller, A. Klehr, Bistability, self-sustained oscillations, and irregular operation of a gaAs laser coupled to an external resonator. Opt. Commun. **47**(4), 297–301 (1983)
46. S. Bauer, O. Brox, J. Kreissl, B. Sartorius, M. Radziunas, J. Sieber, H.-J. Wünsche, F. Henneberger, Nonlinear dynamics of semiconductor lasers with active optical feedback. Phys. Rev. E **69**(1), 016206 (2004)
47. N. Dutta, G. Agrawal, M. Focht, Bistability in coupled cavity semiconductor lasers. Appl. Phys. Lett. **44**(1), 30–32 (1984)
48. A. Pimenov, E.A. Viktorov, S.P. Hegarty, T. Habruseva, G. Huyet, D. Rachinskii, A.G. Vladimirov, Bistability and hysteresis in an optically injected two-section semiconductor laser. Phys. Rev. E **89**, 052903 (2014)
49. U. Bandelow, M. Radziunas, A. Vladimirov, B. Hüttl, R. Kaiser, Harmonic mode-locking in monolithic semiconductor lasers: theory, simulations and experiment. Opt. Quantum Electron. **38**, 495–512 (2006)
50. M. Rossetti, P. Bardella, I. Montrosset, Modeling passive mode-locking in quantum dot lasers: a comparison between a finite-difference traveling-wave model and a delayed differential equation approach. IEEE J. Quantum Electron. **47**(5), 569–576 (2011)
51. M. Born, E. Wolf, *Principles of Optics* (Pergamon Press, Oxford, 1980)